Journal of Catalysis 286 (2012) iii–xi

Contents lists available at SciVerse ScienceDirect

Journal of Catalysis

journal homepage: www.elsevier.com/locate/jcat

Journal of Catalysis Vol. 286, 2012

Contents

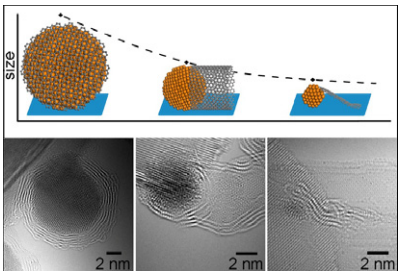

The formation of graphene layers on MgO-supported Pt nanoparticles was studied by both in situ and ex situ high-resolution transmission electron microscopy (HRTEM), which indicate that graphene sheets grow from steps in the surface of Pt nanoparticles and the subsequent morphology of the graphene sheets is a strong function of Pt particle size.

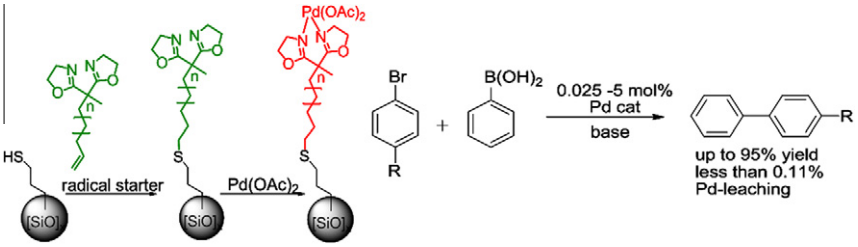

A catalytic system including a $Pd(OAc)_2$-bis(oxazoline) complex bonded to 3-mercaptopropyl-functionalized silica gel is presented. The catalyst was tested for Suzuki–Miyaura reactions. The heterogeneity of the catalytic system was studied indicating that there is virtually no Pd-leaching. Furthermore, the catalyst can be reused multiple times without significant loss of stability or structure.

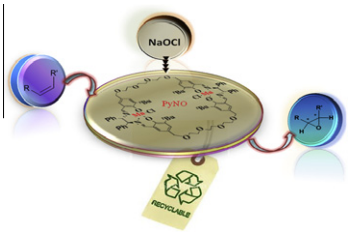

Chiral macrocyclic Mn(III) salen complexes catalyze the enantioselective epoxidation of nonfunctionalized alkenes with sodium hypochlorite in presence of several pyridine-*N*-oxide at 0 °C.

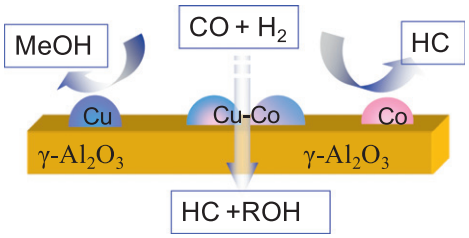

The alumina-supported copper–cobalt catalysts exhibit catalytic performance in carbon monoxide hydrogenation very different from that of monometallic counterparts. The catalytic and characterization results are interpreted in terms of formation of bimetallic particles in the activated catalysts.

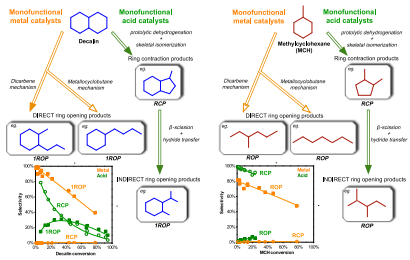

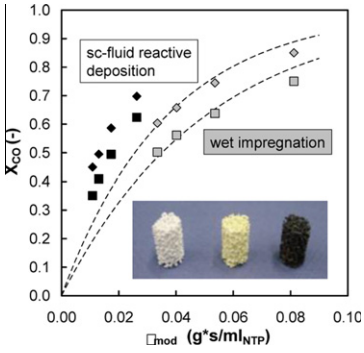

Novel PROX-catalysts on ceramic sponges prepared via supercritical fluid reactive deposition outperform catalysts prepared via conventional routes.

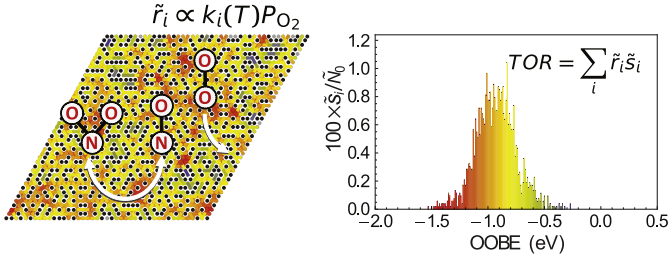

A DFT-based cluster expansion (CE) combined with Monte Carlo simulations is used to accurately describe the heterogeneous distribution of adsorbates and O_2 dissociation sites at a Pt (1 1 1) surface under realistic NO oxidation conditions. O_2 dissociation rates are sensitive to the local arrangement of adsorbates, and averaging over these arrangements provides reaction rates and rate derivatives in good agreement with experiment.

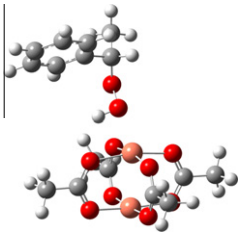

Density functional theory calculations were performed for hydroperoxide decomposition over metal clusters found in metal-organic frameworks. The calculations suggest that in some cases, constraints of the framework prevent metals in the MOF interior from catalyzing this reaction.

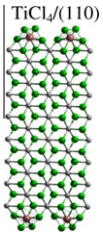

The adsorption of $TiCl_4$ on the surfaces of $MgCl_2$ crystals has been investigated by means of state-of-the-art periodic hybrid DFT methods (B3LYP(-D), PBE0(-D) and M06 approximations). The inclusion of dispersion forces turned out to be crucial for a correct analysis of the problem: the phenomenon is essentially dispersion-driven. Under conditions representative of precatalyst preparation, $TiCl_4$ can only adsorb on $MgCl_2$(1 1 0); with respect to the indication of a preferential binding to $MgCl_2$(1 0 4), the present DFT investigation is negative.

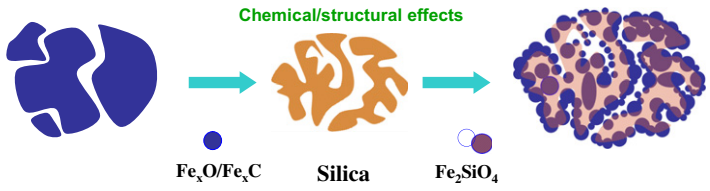

Silica affects iron Fischer–Tropsch catalysts in several ways. As a chemical promoter, it inhibits reduction and carburization of the iron, while in structural sense, it improves the iron dispersion and stabilizes the active phase. Finally, it suppresses the formation of methane.

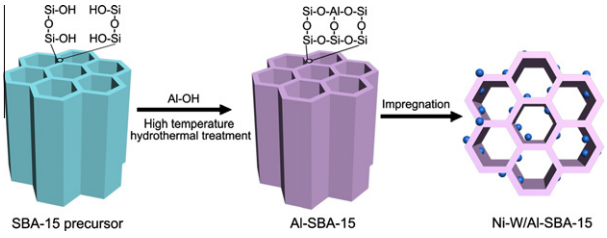

Al-SBA-15 was prepared by adjusting the pH value during high-temperature hydrothermal treatment. Appropriate metal–support interaction combined with suitable acidity endowed the NiW/Al-SBA-15 catalyst with excellent hydrodesulfurization activity.

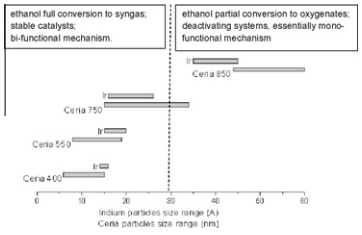

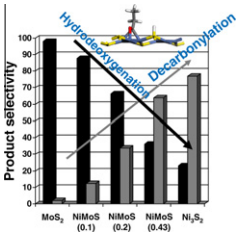

The deoxygenation pathways of ester depend on the nature of the transition metal sulfide bulk catalyst: MoS_2-based catalysts favor hydrodeoxygenation, whereas the decarbonylation selectivity increases as a function of the Ni monosulfide content; a rational interpretation is furnished by DFT calculations.

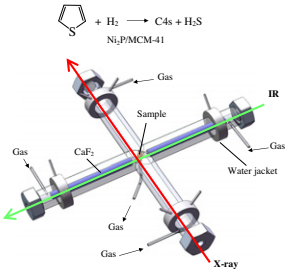

Simultaneous X-ray absorption spectroscopy and transmission Fourier transform infrared spectroscopy were applied to study the mechanism of thiophene hydrodesulfurization over Ni_2P/MCM-41. The measurements were carried out at transient conditions using quick X-ray absorption with a limiting spectral acquisition time of 10 s. The studies showed that a phosphosulfide was the active species and that a tetrahydrothiophene intermediate was involved in the reaction.

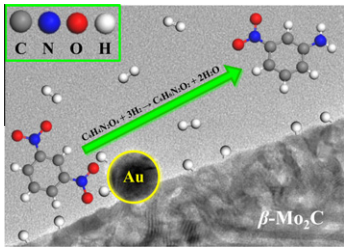

Au/β-Mo_2C promotes hydrogenation of dinitrobenzene with exclusive production of nitroaniline.

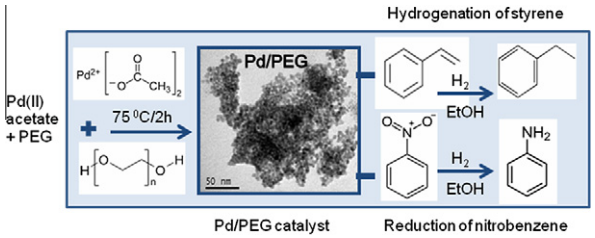

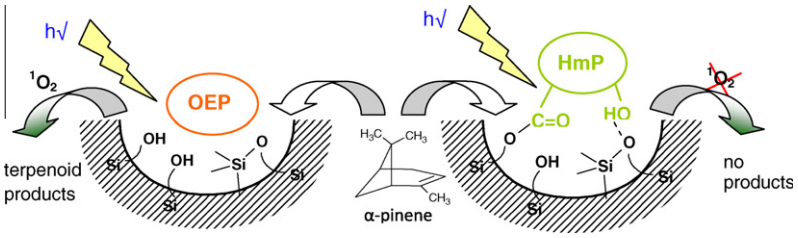

Octaethylporphine (OEP) and hematoporphyrin (HmP) immobilized in pore silica gel show good luminescent properties, but biocatalytic activity in the photoconversion of α-pinene is only found for OEP/SiO_2. It is suggested that the blocking of silanol/siloxane groups by electrophilic substituents of HmP prevents transfer of energy for the formation of reactive oxygen species.

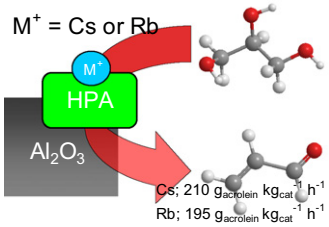

Dehydration of glycerol to acrolein was carried out using rubidium- and caesium-doped silicotungstic acid catalysts supported on alumina. Cs-doped silicotungstic acid supported on theta-delta alumina gave a maximum selectivity of *ca.* 90% at 100% glycerol conversion and with a more concentrated glycerol feed (20 wt.%) achieved an space time yield of 210 $g_{(acrolein)}$ $kg_{(cat)}^{-1}$ h^{-1}. The catalysts were tested for up to 200 h on-stream and found to be stable for 90 h (10 wt.% glycerol).

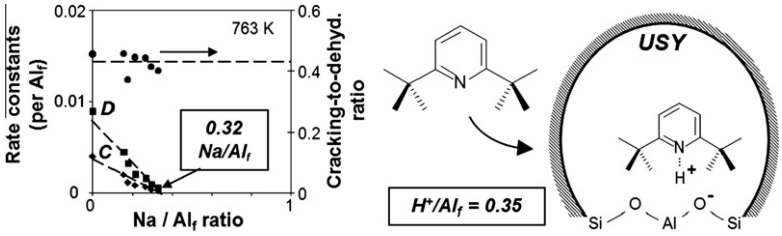

Demystifying faujasite: Isobutane cracking (C) and dehydrogenation (D) rate constants (per framework Al; Al_f), but not their ratio, decreased monotonically with Na^+ content in ultrastable Y (USY) zeolite. Similar Na^+ and 2,6-di-*tert*-butylpyridine titrant uptakes completely suppressed catalytic rates, indicating that there are fewer H^+ sites than Al_f atoms and that Na^+ stoichiometrically replaces H^+ sites that are uniform in reactivity and acid strength.

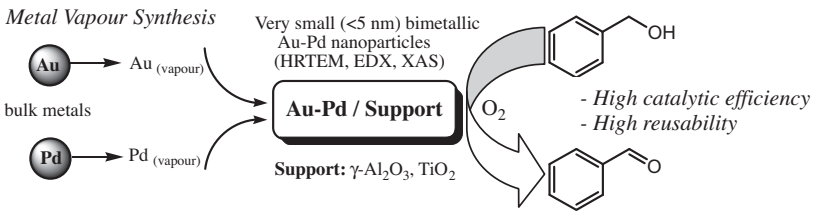

New supported Au–Pd bimetallic catalysts were easily synthesized starting from Au–Pd/acetone solutions generated according to the metal vapour synthesis technique. Transmission electron microscopy (TEM) and X-ray absorption spectroscopy (XAS) analyses on supported systems showed very small (<5 nm) bimetallic Au–Pd nanoparticles and very narrow size distributions. The catalytic efficiency of supported Au–Pd systems was tested in the selective oxidation of benzyl alcohol with molecular oxygen evidencing the role of the structural features on their catalytic activity and selectivity.

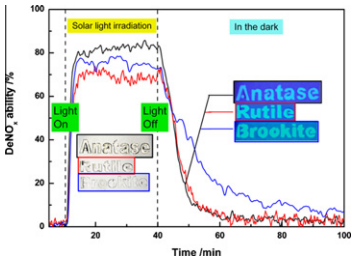

Nitrogen doping of TiO_2 and coupling it with a fluorescent material induces persistent photocatalytic activity even after switching off the light.

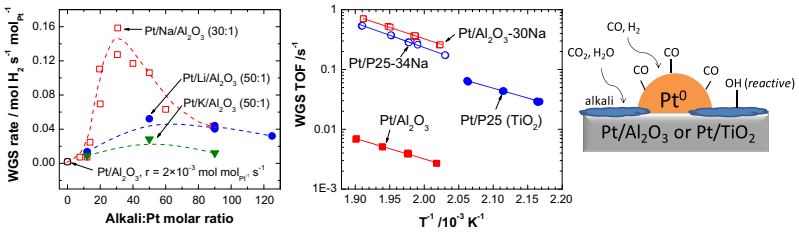

The enhancement of the WGS rate by alkali components (Li, Na, and K) was confirmed on Pt/Al_2O_3. Addition of sodium resulted in the highest promotion. Upon addition of Na, the rate and kinetics of Pt/TiO_2 were similar to Pt/Al_2O_3. Promoted samples showed fully reduced Pt under reaction conditions. The promotion by alkali is therefore caused by the modification of the support and not the nature of Pt.

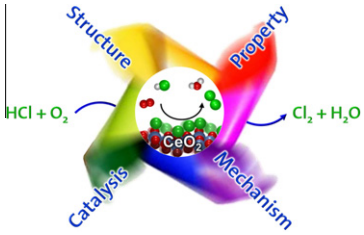

CeO_2 is a promising catalytic system for industrial use in HCl oxidation. Experimental and theoretical studies reveal performance descriptors and provide molecular-level understanding of the reaction over this intriguing oxide.

CORRIGENDA